

Introspective Deep Metric Learning

Chengkun Wang^{1,2,*}, Wenzhao Zheng^{1,2,*},
Zheng Zhu³, Jie Zhou^{1,2}, and Jiwen Lu^{1,2,†}

¹ Beijing National Research Center for Information Science and Technology, China

² Department of Automation, Tsinghua University, China

³ PhiGent Robotics

{wck20,zhengwz18}@mails.tsinghua.edu.cn;
zhengzhu@ieee.org; {jzhou,lujiwen}@tsinghua.edu.cn

Abstract. This paper proposes an introspective deep metric learning (IDML) framework for uncertainty-aware comparisons of images. Conventional deep metric learning methods produce confident semantic distances between images regardless of the uncertainty level. However, we argue that a good similarity model should consider the semantic discrepancies with caution to better deal with ambiguous images for more robust training. To achieve this, we propose to represent an image using not only a semantic embedding but also an accompanying uncertainty embedding, which describes the semantic characteristics and ambiguity of an image, respectively. We further propose an introspective similarity metric to make similarity judgments between images considering both their semantic differences and ambiguities. Our framework attains state-of-the-art performance on the widely used CUB-200-2011, Cars196, and Stanford Online Products datasets for image retrieval. We further evaluate our framework for image classification on the ImageNet-1K, CIFAR-10, and CIFAR-100 datasets, which shows that equipping existing data mixing methods with the proposed introspective metric consistently achieves better results (*e.g.*, +0.44% for CutMix on ImageNet-1K). Code is available at: <https://github.com/wangck20/IDML>.

Keywords: Deep Metric Learning, Uncertainty-Aware Similarity Judgments, Introspective Similarity Metric

1 Introduction

Learning an effective metric to measure the similarity between data is a long-standing problem in computer vision, which serves as a fundamental step in various downstream tasks, such as face recognition [15, 49, 72], image retrieval [1, 53, 88] and image classification [9, 51]. The objective of metric learning is to reduce the distances between positive pairs and enlarge the distances between negative pairs, which has recently powered the rapid developments for both supervised learning [57, 68, 69, 90] and unsupervised learning [4, 6, 14, 18].

* Equal contribution.

† Corresponding author.

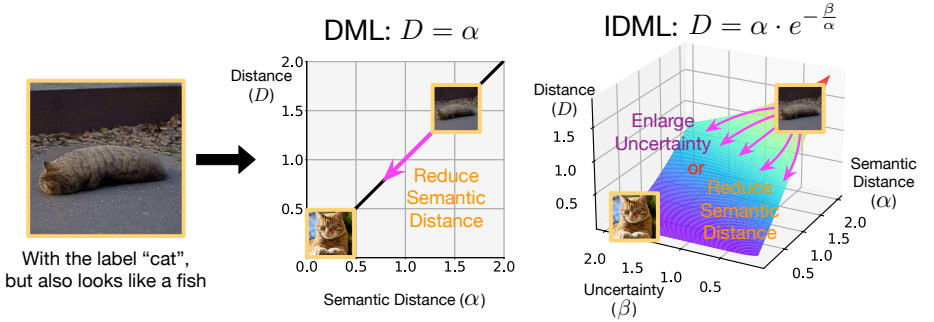


Fig. 1: The motivation of our IDML framework. For a semantically ambiguous image, conventional DML explicitly reduces its distance with other intraclass images unaware of the uncertainty. Differently, the proposed introspective similarity metric provides an alternative way to enlarge the uncertainty level to allow confusion in the network.

Generally, deep metric learning (DML) employs deep neural networks [19, 52, 56] to map an image to a discriminative embedding space [83]. Most methods represent images using a deterministic embedding which only describes the characteristic features [49, 71]. Nevertheless, when asked to classify a certain image, humans are able to additionally provide the corresponding confidence as well as the semantic features of the image since an image might be ambiguous. Motivated by this, researchers have proposed a variety of probabilistic embedding methods using distributions to model images in the embedding space [8, 40, 54, 79]. They typically use KL-divergence [20] or Monte-Carlo-sampling-based [40] distances to measure the similarity between images. They regard the variance of the distributions as the uncertainty measure of images, yet they still provide a confident judgment of similarity regardless of the uncertainty. Specifically, though the variance affects the distribution discrepancy, a larger variance of an image does not necessarily blur its differences from other images. Given a highly ambiguous image (*e.g.*, an extremely blurred image), we think it is more reasonable to weaken the semantic discrepancies and consider it similar to other images since it literally could be anything.

In this paper, we propose an introspective similarity metric to achieve this and further present an introspective deep metric learning (IDML) framework for both image retrieval and classification. Different from existing methods, we represent an image using a semantic embedding to capture the semantic characteristics and further accompany it with an uncertainty embedding to model the uncertainty. An introspective similarity metric then takes as input both embeddings and outputs an uncertainty-aware similarity score, which softens the semantic discrepancies by the degree of uncertainty. Different from the conventional metric, the proposed introspective metric deems a pair of images similar if they are either semantically similar or ambiguous to judge, as illustrated in Fig. 1. It provides more flexibility to the training process to avoid the harmful influence of inaccurately labeled data. To further demonstrate the advantage of the proposed metric for learning with uncertainties, we employ the widely used Mixup [7, 61, 82] technique to generate images with large uncertainties and further employ the IDML framework for learning. The overall framework

of the proposed IDML can be trained efficiently in an end-to-end manner and generally applied to existing deep metric learning methods. We perform extensive experiments on the CUB-200-2011, Cars196, and Stanford Online Products datasets for image retrieval, which shows that our framework generally improves the performance of existing deep metric learning methods by a large margin and attains state-of-the-art results. We also evaluate our framework on the image classification task on the widely used ImageNet-1K, CIFAR-10, and CIFAR-100 datasets. Experimental results show that our introspective similarity metric further boosts existing data mixing methods including Mixup and CutMix [78, 82] (*e.g.*, +0.44% for CutMix on ImageNet-1K).

2 Related Work

Deep Metric Learning: Deep metric learning aims to construct an effective embedding space to measure the similarity between images. The objective is to decrease intraclass distances and increase interclass distances. Most methods [2, 9, 10, 22, 27, 35, 53, 64–67, 74, 80, 85] employ a discriminative loss to learn the image embeddings. For example, the commonly used contrastive loss [22] pulls embeddings from the same class as close as possible while maintaining a fixed margin between embeddings from different classes. Wang *et al.* [67] further formulated three types of similarities between embeddings and proposed a multi-similarity loss to restrict them. The ProxyNCA loss [35] generates a proxy for each class and instead constrains the distances between embeddings and proxies.

In addition to the design of loss functions, various methods have explored effective sampling strategies for better training [13, 17, 49, 71, 77, 78, 82, 86]. For example, hard negative mining [17, 49, 77] selects challenging negative samples for more efficient learning of the metric. To further alleviate the lack of informative training samples, recent works [13, 87] proposed to generate synthetic samples for training. Also, a variety of data augmentation methods improve the performance by mixing original images for better generalization [78, 82]. The aforementioned methods employ synthetic images for training, which are can be semantically ambiguous. We design an introspective similarity metric to consider the uncertainty and further incorporate them to make similarity judgments.

Uncertainty Modeling: Uncertainty modeling is widely adopted in natural language processing to model the inherent hierarchies of words [37, 38, 62]. Vilnis *et al.* [62] proposed the Gaussian formation in word embedding and Nguyen *et al.* [38] presented a mixture model to learn multi-sense word embeddings. The computer vision field has also benefited from uncertainty modeling due to the natural uncertainty in images caused by various factors such as occlusion and blur [26, 50]. Various methods have attempted to model the uncertainty for better robustness and generalization in face recognition [3, 51], point cloud segmentation [79], and age estimation [31].

A prevailing method is to model each image as a statistical distribution and regard the variance as the uncertainty measure. For example, Oh *et al.* [40] employed Gaussian distributions to represent images and used Monte-Carlo sam-

pling to sample several point embeddings from the distributions. They then imposed a soft contrastive loss on the sampled embeddings to optimize the metric. Similar strategy has also been used in pose estimation [54], cross-model retrieval [8] and unsupervised embedding learning [73]. However, they still make confident similarity judgments regardless of the uncertainty and a larger variance would not necessarily weaken the semantic discrepancies between samples. Differently, we propose an introspective metric to measure the similarity between images, which tends to omit the semantic differences between two images given a large uncertainty level. Also, our method bypasses the optimization of distributions and can further increase the robustness of the model.

3 Proposed Approach

In this section, we first revisit existing deterministic and probabilistic deep metric learning methods and introduce the motivation of our framework. We then present the introspective similarity metric and elaborate on the introspective deep metric learning framework. Lastly, we conduct a gradient analysis to reveal the advantage of our framework.

3.1 Motivation of an Uncertainty-Aware Metric

Let \mathbf{X} be an image set with N training samples $\{\mathbf{x}_1, \dots, \mathbf{x}_N\}$ and \mathbf{L} be the ground truth label set $\{l_1, \dots, l_N\}$. Deep metric learning methods aim at learning a mapping to transform each image \mathbf{x}_i to an embedding space, where conventional methods [22, 35] use a deterministic vector embedding \mathbf{y}_i to represent an image. They usually adopt the Euclidean distance as the distance measure:

$$D(\mathbf{x}_1, \mathbf{x}_2) = D_E(\mathbf{x}_1, \mathbf{x}_2) = \|\mathbf{y}_1 - \mathbf{y}_2\|_2, \quad (1)$$

where $\|\cdot\|_2$ denotes the L2-norm. They then impose various constraints on the pairwise distances to enlarge interclass distances and reduce intraclass distances.

Conventional DML methods only represent the semantic information in the embedding space, ignoring the possible uncertainty in images. However, the semantic uncertainty widely exists resulting from low resolution, blur, occlusion, or semantic ambiguity of images, which motivates probabilistic embedding learning approaches [8, 40] to model images as statistical distributions \mathbf{Y} in the embedding space. They further use the distribution variance σ to measure the uncertainty of the image in the embedding space. A widely used method is to employ a Gaussian distribution to describe an image [40], *i.e.*, $\mathbf{Y} \sim N(\mu, \sigma)$, where they use a deep network to learn two vectors μ and σ as the mean and variance of the distribution, respectively, assuming each dimension is independent. They employ distribution divergences [20, 75] or Monte-Carlo-sampling-based [40] distances as the similarity metric. For instance, Hershey *et al.* [20] adopted the KL-divergence to measure the discrepancy of two Gaussian distributions \mathbf{Y}_1 and \mathbf{Y}_2 :

$$D_{KL} = -\frac{1}{2} \sum_{k=1}^d \left[\log \frac{\sigma_{1,k}^2}{\sigma_{2,k}^2} - \frac{\sigma_{1,k}^2}{\sigma_{2,k}^2} - \frac{(\mu_{1,k} - \mu_{2,k})^2}{\sigma_{2,k}^2} + 1 \right], \quad (2)$$

where d denotes the dimension of the Gaussian distributions, $\mathbf{Y}_1 \sim N(\mu_1, \sigma_1)$, and $\mathbf{Y}_2 \sim N(\mu_2, \sigma_2)$, and $\sigma_{1,k}$ denotes the k th component of σ_1 .

One can find that for two distributions with the same mean, their discrepancy solely depends on the ratio of the variance. The discrepancy still varies greatly when the variance of one image is large, *i.e.*, of large uncertainty. In other words, it still provides confident judgments about the similarity even when uncertain. However, we argue that a good similarity metric should weaken the semantic discrepancies for uncertain image pairs to allow confusion during training, which has been proven to be useful in knowledge distillation [21]. This avoids the false pulling of ambiguous pairs to improve the generalization of the learned model.

3.2 Introspective Similarity Metric

To facilitate an uncertainty-aware similarity metric, we first need to model the uncertainty in images. Different from existing probabilistic deep embedding learning methods to model images as distributions, we propose to represent an image using a semantic embedding \mathbf{s} and an uncertainty embedding \mathbf{u} , *i.e.*, $\mathbf{y} = \{\mathbf{s}, \mathbf{u}\}$. The semantic embedding \mathbf{s} describes the semantic characteristics of an image while the uncertainty embedding \mathbf{u} models the ambiguity.

For comparing two images \mathbf{x}_1 and \mathbf{x}_2 , we define the semantic distance as $\alpha(\mathbf{x}_1, \mathbf{x}_2) = \|\mathbf{s}_1 - \mathbf{s}_2\|_2$ similar to conventional DML methods but further compute a similarity uncertainty as $\beta(\mathbf{x}_1, \mathbf{x}_2) = \|\mathbf{u}_1 + \mathbf{u}_2\|_2$. Note that we add the vectors of the uncertainty embeddings before computing the norm instead of directly adding their norms. The reason is that the uncertainty should depend on both concerning images. For example, it might be difficult to differentiate an image from an elephant, but it can be affirmatively distinguished from a person.

When determining the semantic similarity between two images, an introspective metric needs to consider both the semantic distance and the similarity uncertainty. And when not certain enough, the metric refuses to distinguish semantic discrepancies. Formally, we consider it reckless to identify the semantic discrepancy between \mathbf{x}_1 and \mathbf{x}_2 when:

$$\beta(\mathbf{x}_1, \mathbf{x}_2) + \gamma \geq \alpha(\mathbf{x}_1, \mathbf{x}_2), \quad (3)$$

where $\gamma > 0$ is the introspective bias indicating the introspective degree of the metric. The positive value of γ represents that the metric is still suspicious even if the image representation model provides no uncertainty. We then define a strict introspective similarity metric as:

$$\tilde{D}_{IN}(\mathbf{x}_1, \mathbf{x}_2) = \alpha(\mathbf{x}_1, \mathbf{x}_2) \cdot I(\alpha(\mathbf{x}_1, \mathbf{x}_2) - \beta(\mathbf{x}_1, \mathbf{x}_2) - \gamma), \quad (4)$$

where $I(x)$ is an indicator function which outputs 1 if $x > 0$ and 0 otherwise.

However, the use of an indicator function is too strict and hard to optimize during training. We instead compare the semantic distance and the similarity uncertainty to define the relative uncertainty of two images:

$$\text{r_conf}(\mathbf{x}_1, \mathbf{x}_2) = \frac{\beta(\mathbf{x}_1, \mathbf{x}_2) + \gamma}{\alpha(\mathbf{x}_1, \mathbf{x}_2)}. \quad (5)$$

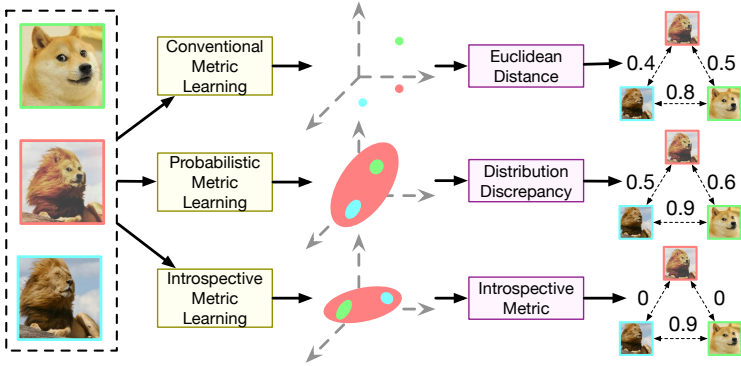


Fig. 2: Comparisons between different similarity metrics. Conventional metric learning and probabilistic metric learning both produce a discriminative distance for a pair of images regardless of the uncertainty level. Our introspective similarity metric weakens the semantic discrepancies for uncertain pairs.

Note that the relative uncertainty is constantly positive. We then use it to soften the semantic discrepancy to obtain our introspective similarity metric:

$$D_{IN}(\mathbf{x}_1, \mathbf{x}_2) = \alpha(\mathbf{x}_1, \mathbf{x}_2) \cdot e^{(-\frac{1}{\tau} \text{r_conf}(\mathbf{x}_1, \mathbf{x}_2))}, \quad (6)$$

$\tau > 0$ is a pre-defined hyperparameter to control the weakening degree. Note that the proposed introspective similarity metric does not satisfy the triangular equation and thus is not a mathematically strict metric. We follow existing work [39, 76] to still refer to it as a metric.

Intuitively, the proposed introspectively metric considers both the semantic distance and the similarity uncertainty between two images to conduct the final semantic discrepancies. It generally produces a smaller distance for two images due to the awareness of the uncertainty. Given two pairs of images with the same semantic distance, the introspective metric distinguishes better for the pair with a smaller similarity uncertainty. Also, when the uncertainty of two images outweighs the semantic distance to a great extent, the introspective metric simply outputs a near-zero semantic distance avoiding unnecessary influence on the network. Fig. 2 presents the comparison between different similarity metrics.

3.3 Introspective Deep Metric Learning

We demonstrate how to apply the proposed introspective metric to existing methods and present the overall framework of IDML, as illustrated in Fig. 3.

The semantic uncertainty naturally exists in images, yet it is hard to accurately describe the uncertainty for each image. Moreover, many data augmentation methods [13, 78, 82] in the literature expand the training data by generating synthetic images, which are known to possess multiple concepts. Specifically, we employ the data mixing strategy [78, 82] to demonstrate the advantage of our framework to deal with data with large uncertainty.

Although data uncertainty naturally exists in original images, we utilize the Mixup [82] method to generate images with larger uncertainty to prove that

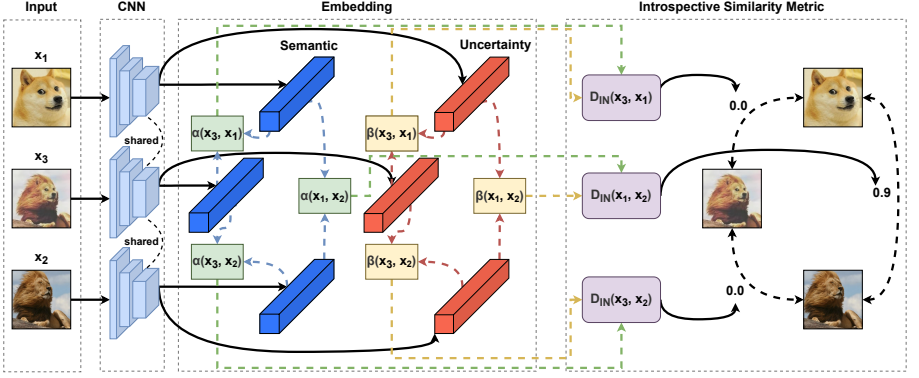


Fig. 3: An illustration of the proposed IDML framework. We employ a convolutional neural network to represent each image by a semantic embedding and an uncertainty embedding. We then use the distance between semantic embeddings as the semantic discrepancy and add the uncertainty embeddings for uncertainty measure. The introspective similarity metric then uses the uncertainty level to weaken the semantic discrepancy to make a discreet similarity judgment.

our framework is capable of processing ambiguous data more effectively and achieving better performances. Specifically, we mix the original images \mathbf{x}_1 and \mathbf{x}_2 to obtain $\mathbf{x}_m = \lambda \cdot \mathbf{x}_1 + (1 - \lambda) \cdot \mathbf{x}_2$. However, different from the Mixup method [82] which combines the labels of two images by $l_m = \lambda \cdot l_1 + (1 - \lambda) \cdot l_2$, we treat l_m as a set which simultaneously includes l_1 and l_2 , noted as $l_m = \{l_1, l_2\}$. On such condition, we define $l_i = l_j$ if $l_i \cap l_j \neq \emptyset$ and $l_i \neq l_j$ otherwise. We adopt the convolutional network to extract the feature embeddings of both original images and mixed images $\mathbf{y}_i = f(\mathbf{x}_i) = \{\mathbf{s}_i, \mathbf{u}_i\}$, where \mathbf{s}_i and \mathbf{u}_i denote the semantic feature embedding and the uncertainty feature embedding of \mathbf{x}_i , respectively.

The similarity computation of paired samples follows our introspective similarity metric. In addition, our introspective similarity is compatible with a variety of loss formulations. For example, we can employ the margin loss with the distance-weighted sampling strategy [71] to optimize the pairwise distances:

$$J_m(\mathbf{y}, \mathbf{L}) = \sum_{l_i=l_j} [D_{IN}(\mathbf{x}_i, \mathbf{x}_j) - \xi]_+ - \sum_{l_i \neq l_j} I(p(D_{IN}(\mathbf{x}_i, \mathbf{x}_j))) [\omega - D_{IN}(\mathbf{x}_i, \mathbf{x}_j)]_+, \quad (7)$$

where $D_{IN}(\mathbf{x}_i, \mathbf{x}_j)$ follows (6), the random variable $I(p)$ has a probability of p to be 1 and 0 otherwise, $p(d) = \min(\phi, d^{2-n} [1 - \frac{1}{4} d^2]^{\frac{3-n}{2}})$, $[\cdot]_+ = \max(\cdot, 0)$, ξ and ω are two pre-defined margins, and ϕ is a positive constant.

In addition, proxy-based losses such as the softmax loss [9, 55] fits our similarity metric as well. It should be noted that different from the Euclidean distance, various proxy-based losses compute the cosine similarity $C(\mathbf{x}_i, \mathbf{p}_j)$ between an image \mathbf{x}_i and a class-level representative \mathbf{p}_j . Therefore, we conduct the confidence decay of the semantic similarity in another way:

$$C_{IN}(\mathbf{x}_i, \mathbf{p}_j) = 1 - (1 - C(\mathbf{x}_i, \mathbf{p}_j)) \cdot e^{(-\frac{1}{\tau} \text{r_conf}(\mathbf{x}_i, \mathbf{p}_j))}, \quad (8)$$

where $r_conf(\mathbf{x}_i, \mathbf{p}_j)$ denotes the relative uncertainty between the image and the representative, and we provide the softmax loss based on our similarity metric:

$$J_s(\mathbf{y}, \mathbf{L}) = \frac{1}{N} \sum_{i=1}^N \left(-\log \frac{\sum_{l_{\mathbf{p}_j}=l_i} e^{C_{IN}(\mathbf{x}_i, \mathbf{p}_j)}}{\sum_{l_{\mathbf{p}_j} \neq l_i} e^{C_{IN}(\mathbf{x}_i, \mathbf{p}_j)}} \right), \quad (9)$$

where $l_{\mathbf{p}_j}$ is the category of the class representative \mathbf{p}_j .

For inference, we directly use the Euclidean distance between semantic embeddings as the similarity metric and can optionally use the uncertainty embedding to indicate the uncertainty level.

3.4 Gradient Analysis

We provide a gradient analysis to demonstrate the effect of our introspective similarity metric on the learning of semantic embeddings. Intuitively, our proposed similarity metric results in reduced semantic discrepancies to impose fewer influences for uncertain samples. Therefore, we present a detailed gradient analysis of the parameters of the semantic embedding layer W^t with the Euclidean-distance-based methods for example. Firstly, we formulate the backpropagation process in the t -th iteration as follows:

$$\frac{\partial J}{\partial W^t} = \frac{\partial J}{\partial \mathbf{S}} \cdot \frac{\partial \mathbf{S}}{\partial W^t} = \frac{\partial J}{\partial D_{IN}} \cdot \frac{\partial D_{IN}}{\partial \mathbf{S}} \cdot \frac{\partial \mathbf{S}}{\partial W^t}, \quad (10)$$

where J and \mathbf{S} denote the loss function and the semantic embeddings for simplicity. Actually, the partial term $\frac{\partial J}{\partial D_{IN}}$ depends on the form of the loss function while $\frac{\partial \mathbf{S}}{\partial W^t}$ is merely relevant to the architecture of the network. On such condition, $\frac{\partial D_{IN}}{\partial \mathbf{S}}$ contributes to the update level of the parameters, and a larger gradient undoubtedly represents a larger update. Next, we formulate the above gradient based on a paired samples $\{\mathbf{y}_1 = (\mathbf{s}_1, \mathbf{u}_1), \mathbf{y}_2 = (\mathbf{s}_2, \mathbf{u}_2)\}$, which is as follows: (D_{IN} is the same as (6) and we set $\tau = 1$ and $\gamma = 0$ for simplicity.)

$$H(\mathbf{u}_1, \mathbf{u}_2) = \frac{\partial D_{IN}(\mathbf{x}_1, \mathbf{x}_2)}{\partial \mathbf{s}_1} = \frac{\partial \|\mathbf{s}_1 - \mathbf{s}_2\|_2}{\partial \mathbf{s}_1} \cdot e^{-\frac{\|\mathbf{u}_1 + \mathbf{u}_2\|_2}{\|\mathbf{s}_1 - \mathbf{s}_2\|_2}} \cdot \left(1 + \frac{\|\mathbf{u}_1 + \mathbf{u}_2\|_2}{\|\mathbf{s}_1 - \mathbf{s}_2\|_2}\right) \quad (11)$$

where $H(\mathbf{u}_1, \mathbf{u}_2)$ is a function of $\{\mathbf{u}_1, \mathbf{u}_2\}$ if the semantic feature embeddings $\{\mathbf{s}_1, \mathbf{s}_2\}$ are fixed, $\frac{\partial \|\mathbf{s}_1 - \mathbf{s}_2\|_2}{\partial \mathbf{s}_1}$ denotes the gradient for the original Euclidean distance form, and $e^{-\frac{\|\mathbf{u}_1 + \mathbf{u}_2\|_2}{\|\mathbf{s}_1 - \mathbf{s}_2\|_2}} \cdot \left(1 + \frac{\|\mathbf{u}_1 + \mathbf{u}_2\|_2}{\|\mathbf{s}_1 - \mathbf{s}_2\|_2}\right)$ connects with the commonly used monotone decreasing function $g(x) = e^{-x} \cdot (1 + x)$ when $x > 0$, which remains decreasing when $\mathbf{u}_1 > 0$.

Therefore, $H(\mathbf{u}_1, \mathbf{u}_2)$ decreases when the length of the uncertainty embedding \mathbf{u}_1 increases. It indicates that images with more uncertainty result in smaller gradients, thus imposing fewer influences on the network. Specially, when $\|\mathbf{u}_1 + \mathbf{u}_2\|_2 = 0$, denoting the absolute certainty of samples, $H(\mathbf{u}_1, \mathbf{u}_2) = \frac{\partial \|\mathbf{s}_1 - \mathbf{s}_2\|_2}{\partial \mathbf{s}_1}$, turning back to the form of the original Euclidean gradient. It denotes that our similarity metric maintains the original judgment for certain samples.

Table 1: Experimental results (%) on the CUB-200-2011, Cars196, and Stanford Online Products datasets compared with state-of-the-art methods. * denotes our reproduced results under the same settings.

Methods	Setting	CUB-200-2011					Cars196					Stanford Online Products				
		R@1	R@2	NMI	RP	M@R	R@1	R@2	NMI	RP	M@R	R@1	R@10	NMI	RP	M@R
SoftTriple [43]	512BN	65.4	76.4	69.3	-	-	84.5	90.7	70.1	-	-	78.3	90.3	92.0	-	-
MIC [44]	128R	66.1	76.8	69.7	-	-	82.6	89.1	68.4	-	-	77.2	89.4	90.0	-	-
DR [34]	512BN	66.1	77.0	-	-	-	85.0	90.5	-	-	-	-	-	-	-	-
HORDE [24]	512BN	66.3	76.7	-	-	-	83.9	90.3	-	-	-	80.1	91.3	-	-	-
ProxyGML [91]	512BN	66.6	77.6	69.8	-	-	85.5	91.8	72.4	-	-	78.0	90.6	90.2	-	-
RankMI [25]	128R	66.7	77.2	71.3	-	-	83.3	89.8	69.4	-	-	74.3	87.9	90.5	-	-
CircleLoss [55]	512R	66.7	77.4	-	-	-	83.4	89.8	-	-	-	78.3	90.5	-	-	-
PADS [45]	128BN	67.3	78.0	69.9	-	-	83.5	89.7	68.8	-	-	76.5	89.0	89.9	-	-
DRO [42]	512BN	68.1	78.4	-	-	-	86.4	91.9	-	-	-	-	-	-	-	-
DIML [84]	512R	68.2	-	-	37.9	26.9	87.0	-	-	39.0	29.4	79.3	-	-	46.4	43.2
DCML [88]	512R	68.4	77.9	71.8	-	-	85.2	91.8	73.9	-	-	79.8	90.8	90.8	-	-
D & C [48]	512R	68.4	78.7	69.7	-	-	87.8	92.5	70.7	-	-	80.3	90.2	-	-	-
DRML [89]	512BN	68.7	78.6	69.3	-	-	86.9	92.1	72.1	-	-	79.9	90.7	90.1	-	-
DiVA [33]	512R	69.2	79.3	71.4	-	-	87.6	92.9	72.2	-	-	79.6	91.2	90.6	-	-
SEC [81]	512BN	69.8	79.4	72.9	-	-	85.7	92.0	74.0	-	-	78.7	90.8	91.9	-	-
MemVir [28]	512BN	69.0	79.2	-	-	-	86.8	92.4	-	-	-	80.0	91.0	-	-	-
P-NCA++ [58]	512R	69.0	79.8	73.9	-	-	86.5	92.5	73.8	-	-	80.7	92.0	-	-	-
NIR [46]	512R	70.5	80.6	72.5	-	-	89.1	93.4	75.0	-	-	80.7	91.5	90.9	-	-
Triplet-SH* [49]	512R	63.6	75.5	67.9	35.1	24.0	70.8	81.7	64.8	31.7	21.1	76.5	89.1	89.7	51.3	48.4
IDML-TSH	512R	65.3	76.5	69.5	36.2	25.0	73.7	84.0	67.3	33.8	24.1	77.4	89.4	90.1	51.9	49.0
ProxyNCA* [35]	512R	64.6	75.6	69.1	35.5	24.7	82.6	89.0	66.4	33.5	23.5	77.0	89.1	89.5	51.9	49.0
IDML-PN	512R	66.0	76.4	70.1	36.5	25.4	85.5	91.3	69.0	36.1	26.4	78.3	90.1	89.9	53.0	49.9
FastAP* [2]	512R	65.1	75.4	68.5	35.9	24.1	81.6	88.5	68.8	35.1	25.2	75.9	89.2	89.7	50.1	46.8
IDML-FAP	512R	66.4	76.4	69.7	36.7	25.5	83.9	89.9	71.9	36.5	26.7	76.8	89.7	90.9	50.9	47.9
Contrastive* [22]	512R	65.6	76.5	68.9	36.5	24.7	82.7	89.6	69.5	35.8	25.7	76.4	88.5	88.9	50.9	47.9
IDML-Con	512R	67.2	77.6	71.3	37.5	25.7	85.5	91.5	72.5	38.8	29.0	77.3	89.7	90.0	51.7	48.5
Margin-DW* [71]	512R	65.9	77.0	69.5	36.0	24.9	82.6	88.7	69.3	36.4	26.5	78.5	89.9	90.1	53.4	50.2
IDML-MDW	512R	67.9	78.3	72.1	37.2	26.1	86.1	91.7	77.3	0.39	2.29	79.4	90.6	91.0	53.7	50.4
Multi-Sim* [67]	512R	67.3	78.2	72.7	36.6	25.5	83.3	90.9	72.2	37.4	27.4	78.1	90.0	89.9	52.9	49.9
IDML-MS	512R	69.0	79.5	73.5	38.5	27.2	86.3	92.2	74.1	40.0	30.8	79.7	91.4	91.2	53.7	50.9
ProxyAnchor* [27]	512R	69.0	79.4	72.3	38.5	27.5	87.3	92.7	75.7	40.9	31.8	79.5	91.1	91.0	53.7	50.5
IDML-PA	512R	70.7	80.2	73.5	39.3	28.4	90.6	94.5	76.9	42.6	33.8	81.5	92.7	92.3	54.8	51.3

4 Experiments

In this section, we conducted various experiments to evaluate the performance of our IDML framework on both image retrieval and classification. We show that employing the proposed introspective similarity metric consistently improves the performance of existing deep metric learning and data mixing methods. We also provide in-depth analyses of the effectiveness of our framework. We conducted all experiments using the PyTorch [41] library.

4.1 Settings

Image Retrieval: We first evaluated our framework under the conventional deep metric learning setting [53, 67] and conducted experiments on three widely-

Table 2: Experimental results (%) of the proposed IDML with ResNet-50 on the ImageNet-1K, CIFAR-10, and CIFAR-100 datasets.

Methods	ImageNet-1K		CIFAR-100		CIFAR-10
	Top-1 Acc	Top-5 Acc	Top-1 Acc	Top-5 Acc	Top-1 Acc
Baseline	76.32	92.95	83.55	96.31	96.15
ISM-Baseline	76.94 (+0.62)	93.24 (+0.29)	84.08 (+0.53)	96.46 (+0.17)	96.43 (+0.28)
Mixup [82]	77.42	93.60	84.22	95.96	96.91
IDML-Mixup	77.95 (+0.53)	93.93 (+0.33)	84.59 (+0.37)	96.79 (+0.83)	97.13 (+0.22)
Cutmix [78]	78.60	94.08	85.53	97.03	97.12
IDML-Cutmix	79.04 (+0.44)	94.47 (+0.39)	85.65 (+0.12)	97.21 (+0.18)	97.32 (+0.20)

used datasets: CUB-200-2011 [63], Cars196 [29], and Stanford Online Products [53]. We provide the detailed dataset splits in the appendix. We adopted the ImageNet [47] pre-trained ResNet-50 [19] as the backbone and two randomly initialized fully connected layers to obtain the semantic embedding and uncertainty embedding, respectively. We set the embedding size to 512 for the main experiments. The training images were first resized to 256×256 and then augmented with random cropping to 224×224 as well as random horizontal flipping with the probability of 50%. We employed Mixup [82] for our framework to generate images with large uncertainty for training. We fixed the batch size to 120 and used the AdamW optimizer with the learning rate of 10^{-5} . We set $\gamma = 3$ for the Cars196 dataset and $\gamma = 0$ for the other datasets and fixed $\epsilon = 5$ for all the datasets during training. We adopted the original similarity metric without our uncertainty-aware term for testing. The reported evaluation metrics include Recall@Ks, normalized mutual information (NMI), R-Precision (RP), and Mean Average Precision at R (M@R). See Musgrave *et al.* [36] for more details.

Image Classification: We evaluated our framework for the image classification task on three datasets: ImageNet-1K [47], CIFAR-10 [30], and CIFAR-100 [30]. The dataset splits are detailed in the appendix as well. We directly implemented the proposed introspective similarity metric on Mixup [82] and CutMix [78] using the official code¹ and used the same hyperparameter without tuning. Specifically, for ImageNet-1K, we adopted the ResNet-50 [19] as the base model and fixed the probability of the Mixup and CutMix to 1.0. We set the batch size to 256 and the total training epochs to 300. The learning rate was initialized to 0.1 and decayed by 0.1 at epochs 75, 150, and 225. For CIFAR-10 and CIFAR-100, we adopted the PyramidNet-200 [16] as the backbone and fixed the probability of the Mixup and Cutmix to 0.5 during training. We set the batch size to 64 and the total training epochs to 300. The learning rate was 0.25 with a 0.1 decay rate at epochs 150 and 225. We used $\gamma = 0$ and $\tau = 1$ for our introspective similarity metric on all datasets.

4.2 Image Retrieval

We evaluated the proposed IDML framework under the conventional deep metric learning setting and compared it with state-of-the-art methods. To demonstrate

¹ <https://github.com/clovaai/CutMix-PyTorch>

Table 3: Analysis of different components of IDML on the CUB-200-2011, Cars196, and Stanford Online Products datasets.

Methods	CUB-200-2011				Cars196				Stanford Online Products			
	R@1	NMI	RP	M@R	R@1	NMI	RP	M@R	R@1	NMI	RP	M@R
Margin-DW [71]	65.9	69.5	36.0	24.9	82.6	69.3	36.4	26.5	78.5	90.1	53.4	50.2
Mixup-MDW	67.1	71.6	36.7	25.5	84.7	72.4	38.0	28.0	79.1	90.5	53.6	50.4
ISM-MDW	67.0	71.4	36.9	25.7	84.4	71.9	37.9	28.1	78.9	90.4	53.6	50.3
PEL [40]-MDW	63.3	67.1	34.6	24.2	80.4	67.1	34.8	25.5	76.4	88.7	51.2	48.7
PEL-Mixup-MDW	64.5	68.6	35.3	24.7	82.3	68.9	35.9	26.1	77.2	89.4	52.1	49.3
IDML-MDW	67.9	72.1	37.2	26.1	86.1	73.0	39.2	29.7	79.4	91.0	53.7	50.4
ProxyAnchor [27]	69.0	72.3	38.5	27.5	87.3	75.7	40.9	31.8	79.5	91.0	53.7	50.5
Mixup-PA	69.8	73.0	39.1	28.1	88.5	75.8	41.0	32.1	80.6	91.8	54.4	50.7
ISM-PA	69.5	73.1	38.9	28.0	88.8	75.8	41.2	32.2	80.3	91.8	54.3	50.9
PEL-PA	64.9	67.1	34.5	23.7	83.4	66.4	34.4	24.9	76.8	89.7	51.8	48.7
PEL-Mixup-PA	65.7	68.0	35.6	24.7	84.5	66.6	34.6	25.1	77.9	90.5	52.6	49.9
IDML-PA	70.7	73.5	39.3	28.4	90.6	76.9	42.6	33.8	81.5	92.3	54.8	51.3

the versatility of our framework, we applied the introspective similarity metric to various loss functions, including the triplet loss with the semi-hard sampling (Triplet-SH) [49], the ProxyNCA loss [35], the FastAP loss [2], the contrastive loss [22], the margin loss with the distance-weighted sampling (Margin-DW) [71], the multi-similarity loss (Multi-Sim) [67], and the ProxyAnchor loss [27].

Table 1 shows the experimental results on the CUB-200-2011 [63], Cars196 [29], and Stanford Online Products [53] datasets. The n-BN/R denotes the model setting where n is the embedding size and BN, R represents BN-Incertion [23] and ResNet-50 [19], respectively. The bold numbers highlight the improvement of our framework compared with the original method, and the red numbers indicate the best results. We observe that our framework achieves a constant performance boost to all the associated methods. Furthermore, we attain state-of-the-art performance on all three datasets by applying our framework to the ProxyAnchor loss, which surpasses the original performance by 3.3% at Recall@1 and 2.0% at M@R on the Cars196 dataset, respectively. This is because the proposed similarity metric is aware of the data uncertainty in images so that the uncertain samples only provide limited training signals.

4.3 Image Classification

For the image classification task, we applied our framework to the widely used Mixup [5] and CutMix [78] methods to evaluate the effectiveness. Table 2 shows the experimental results on the ImageNet-1K [47], CIFAR-10 [30], and CIFAR-100 [30] datasets. The bold numbers highlight the improvement of our framework and the red numbers denote the best results. We first applied the proposed introspective similarity metric (ISM) to the baseline vanilla method without using any data mixing methods. We see consistent performance improvements on all datasets, which demonstrate the significance of exploiting the natural ambiguity in the original images. We also observe that our framework can further improve the data mixing method at top-1 and top-5 accuracy. In particular, the IDML

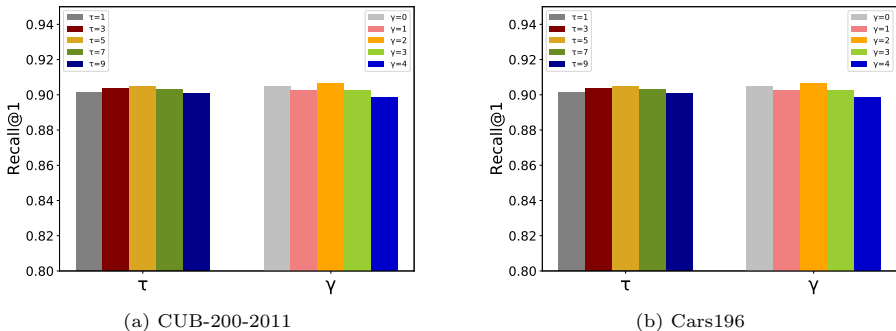


Fig. 4: Impact of metric parameters on the CUB-200-2011 and Cars196 datasets.

framework with Mixup outperforms the original method by 0.53%, 0.37%, and 0.22% at top-1 accuracy on ImageNet-1K, CIFAR-100, and CIFAR-10, respectively. In addition, we improve CutMix by 0.44% on ImageNet-1K and attain a top-1 accuracy of 79.04% using the same recipe. Despite no hyperparameter tuning, this is already a highly competitive performance for a vanilla ResNet-50 using a regular training recipe without extra data or distillation. We provide a performance comparison of different recipes including recent advances [11, 32, 70] in the appendix.

4.4 Analysis

We conducted extensive experiments under the conventional deep metric setting to analyze the effectiveness of our framework.

Ablation Study of Different Components: We conducted experiments with the margin loss and ProxyAnchor loss to analyze the effect of different components of our framework. Table 3 shows the experimental results on the CUB-200-2011, Cars196, and Stanford Online Products datasets.

We first applied Mixup to the baseline method (Mixup-MDW) without using our introspective similarity metric and then only employed the proposed metric without mixup (ISM-MDW). We see that the Mixup method and the proposed ISM can independently boost the performances of the baseline method. Our IDML framework further improves the performance by combining Mixup and our ISM. Furthermore, we reproduced the probabilistic embedding learning (PEL) framework [40] on each loss (PEL-MDW) and also equipped it with Mixup (PEL-Mixup-MDW) for fair comparisons with our framework. We observe that it achieves lower performance than the baseline method, and further using Mixup improves the performance. The performance drop might result from the compromise of discriminativeness when representing images as distributions. Differently, our framework uses an uncertainty embedding to model the uncertainty which does not affect the discriminativeness of the semantic embedding.

Effect of the Hyper-parameters γ and τ : γ determines the introspective bias and τ controls the weakening degree in our introspective similarity metric. They jointly affect the final performance of our framework. We experimentally

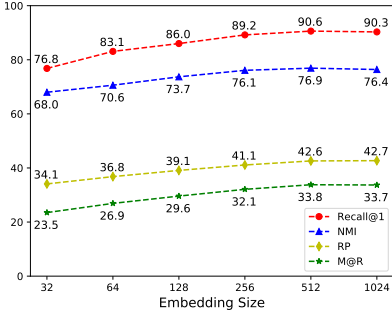


Fig. 5: Effect of the embedding size on the Cars196 dataset.

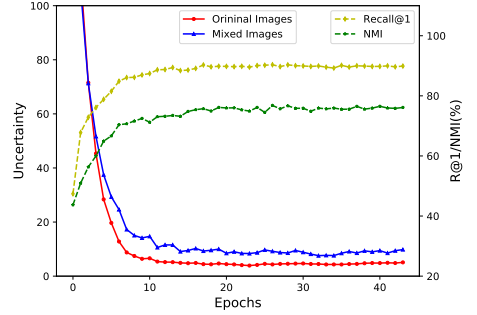


Fig. 6: Uncertainty trend during training on the Cars196 dataset.

evaluated their impacts on the CUB-200-2011 and Cars196 datasets, as demonstrated in Fig. 4. We first fixed γ to 0 and set τ to 1, 3, 5, 7, 9. We see that our framework achieves the best recall@1 when $\tau = 5$ for both datasets, indicating the favor of a modest weakening degree. In addition, we fixed $\tau = 5$ and set γ to 0, 1, 2, 3, 4 for training. The experimental results vary on the two datasets. Specifically, our framework achieves the best performance when $\gamma = 0$ on the CUB-200-2011 dataset while $\gamma = 3$ on the Cars196 dataset. This indicates that the metric is more discreet when comparing images on the Cars196 dataset.

Effect of the Embedding Size: We provided the experimental results with different embedding sizes on the Cars196 dataset in Fig. 5. We observe that the performance surpasses existing methods when the embedding size reaches 256, indicating the superiority of our framework. See more results in the appendix.

Uncertainty Trend during Training: To demonstrate that our IDML framework properly handles mixed images with high uncertainty, we visualize the trend of uncertainty level for both original images and mixed images during training, as shown in Fig. 6. We define the uncertainty level of an image to be the L2-norm of its uncertainty embedding. We see that the uncertainty decreases for both original and mixed images as the training proceeds and becomes stable as the model converges. We also observe that the uncertainty level for mixed images is larger than that of original images. This verifies that our framework can indeed learn the uncertainty in images.

Qualitative Analysis of the Learning Process: We provide a t-SNE [60] visualized analysis of how embeddings are learned using a toy example on the Cars196 dataset in Fig. 7. We visualized the embeddings before and after updating the model with one gradient step. For a dark (and ambiguous) image \mathbf{x}_α , the original method pulls it quite closer to the positive sample \mathbf{x}_p , while the proposed IDML is more cautious and only slightly pulls it together due to the uncertainty to prevent the influence of possible noise.

Uncertainty Levels on the Test Split: We visualize the uncertainty levels on the test split of the CUB-200-2011 and Cars196 datasets, as shown in Fig. 8. We obtain the uncertainty levels of the mixed images together with original images in the test set after the model converges. We observe that the uncertainty of mixed images is much larger than that of the original test images since the mixed images contain the information of two images. Also, we see that several

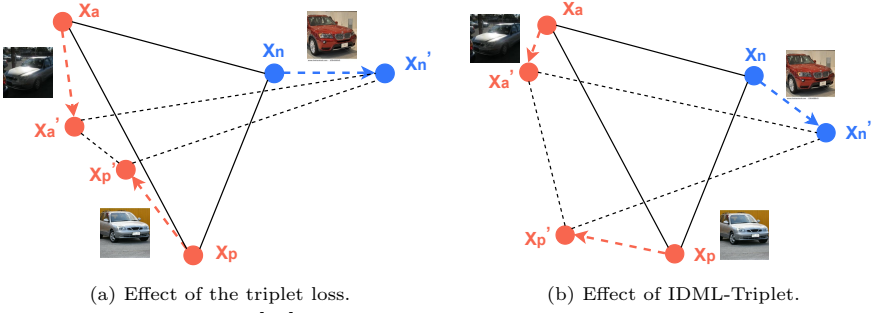


Fig. 7: T-SNE [60] analysis of one-step updating of embeddings.

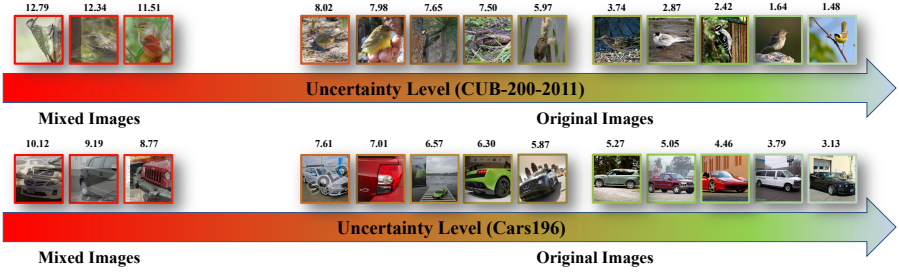


Fig. 8: Uncertainty levels produced by the proposed IDML framework on the test split of CUB-200-2011 and Cars196.

original images result in relatively higher uncertainty than others because of the natural noise such as occlusion and improper directions. This further verifies that the proposed framework can successfully learn the uncertainty in images.

Further Analysis: We provide more experimental results in the appendix including the application of our method on ViTs [59], the effect of using introspective similarity metric during testing, the effect of metric formulations, the effect of batch sizes, the effect of embedding sizes, and more.

5 Conclusion

In this paper, we have presented an introspective deep metric learning (IDML) framework to properly process the data uncertainty for better performance. We have represented an image with a semantic embedding and an uncertainty embedding to model the semantic characteristics and the uncertainty, respectively. We have further proposed an introspective similarity metric to compute an uncertainty-aware similarity score, which weakens semantic discrepancies for uncertain images. We have performed various experiments on the widely-used benchmark datasets on both image retrieval and image classification to analyze the effectiveness of the proposed framework. Experimental results have demonstrated a constant performance boost to various methods in different settings. It is interesting to apply our framework to self-supervised learning and vision transformers as future works.

Appendix

A Implementation for Different Loss Functions

We elaborate on how to apply our IDML framework to various loss functions.

A.1 Triplet Loss

The triplet loss [49] requires a distance ranking within triplets and maintains a margin between positive pairs and negative pairs. The IDML with the triplet loss can be formulated as follows:

$$J_t(\mathbf{y}, \mathbf{L}) = \sum_{a,p,n} [D_{IN}(\mathbf{x}_a, \mathbf{x}_p) - D_{IN}(\mathbf{x}_a, \mathbf{x}_n) + \delta]_+, \quad (12)$$

where $D_{IN}(\cdot)$ denotes our introspective similarity metric, $\{a, p, n\}$ denote the indices of all the possible triplets, $[\cdot]_+ = \max(\cdot, 0)$, and δ is a pre-defined margin. Furthermore, we employ the semi-hard negative sampling strategy to select challenging samples while avoiding noisy ones to boost training. Given an anchor \mathbf{x}_a and a positive sample \mathbf{x}_p , we select the negative sample \mathbf{x}_n which satisfies the following constraint:

$$\mathbf{n}_{a,p}^* = \arg \min_{n: D_{IN}(\mathbf{x}_a, \mathbf{x}_p) < D_{IN}(\mathbf{x}_a, \mathbf{x}_n)} D_{IN}(\mathbf{x}_a, \mathbf{x}_n). \quad (13)$$

A.2 ProxyNCA Loss

The ProxyNCA loss [35] optimizes the distances between a sample and all the proxies:

$$J_p(\mathbf{y}, \mathbf{L}) = \sum_i (-\log \frac{\sum_{l_p=l_i} e^{D_{IN}(\mathbf{x}_i, \mathbf{p})}}{\sum_{l_p \neq l_i} e^{D_{IN}(\mathbf{x}_i, \mathbf{p})}}), \quad (14)$$

where l_i denotes the corresponding label of \mathbf{x}_i , and l_p is the category of \mathbf{p} .

A.3 Contrastive Loss

The contrastive loss [22] directly pulls closer samples from the same class and pushes away negative samples:

$$J_{con}(\mathbf{y}, \mathbf{L}) = \sum_{l_i=l_j} D_{IN}(\mathbf{x}_i, \mathbf{x}_j) + \sum_{l_i \neq l_j} [\delta - D_{IN}(\mathbf{x}_i, \mathbf{x}_j)]_+, \quad (15)$$

where δ is the margin.

A.4 Multi-Similarity Loss

The multi-similarity (MS) loss [67] uses the cosine similarity to measure the relations between samples. We first define the introspective similarity as follows:

$$C_{IN}^*(\mathbf{x}_i, \mathbf{x}_j) = \begin{cases} C_{IN}(\mathbf{x}_i, \mathbf{x}_j), & C_{IN}(\mathbf{x}_i, \mathbf{x}_j) > \min_{l_k=l_i} C_{IN}(\mathbf{x}_i, \mathbf{x}_k) - \epsilon, \\ C_{IN}(\mathbf{x}_i, \mathbf{x}_j), & C_{IN}(\mathbf{x}_i, \mathbf{x}_j) < \max_{l_k \neq l_i} C_{IN}(\mathbf{x}_i, \mathbf{x}_k) - \epsilon, \\ 0, & \text{otherwise,} \end{cases} \quad (16)$$

where ϵ is a hyperparameter. We then instantiate the IDML framework with the MS loss as follows:

$$J_{MS}(\mathbf{y}, \mathbf{L}) = \frac{1}{N} \sum_{i=1}^N \left\{ \frac{1}{\alpha} \log \left[1 + \sum_{l_i=l_j} e^{-\alpha(C_{IN}^*(\mathbf{x}_i, \mathbf{x}_j) - \lambda)} \right] \right. \\ \left. + \frac{1}{\beta} \log \left[1 + \sum_{l_i \neq l_j} e^{\beta(C_{IN}^*(\mathbf{x}_i, \mathbf{x}_j) - \lambda)} \right] \right\}, \quad (17)$$

where α , β , and λ are hyperparameters.

A.5 ProxyAnchor Loss

The ProxyAnchor loss [27] takes advantage of both sample-sample and sample-proxy relations with the cosine similarity to improve the discriminativeness of the embedding space. Our IDML framework can be implemented for the ProxyAnchor loss as follows:

$$J_{pa}(\mathbf{y}, \mathbf{L}) = \frac{1}{|\mathbf{P}^+|} \sum_{\mathbf{p} \in \mathbf{P}^+} \log \left(1 + \sum_{l_i=l_{\mathbf{p}}} e^{-\alpha(C_{IN}(\mathbf{x}_i, \mathbf{p}) - \delta)} \right) \\ + \frac{1}{|\mathbf{P}|} \sum_{\mathbf{p} \in \mathbf{P}} \log \left(1 + \sum_{l_i \neq l_{\mathbf{p}}} e^{\alpha(C_{IN}(\mathbf{x}_i, \mathbf{p}) + \delta)} \right), \quad (18)$$

where \mathbf{P} denotes the set of all proxies, \mathbf{P}^+ denotes the set of positive proxies, $|\cdot|$ represents the size of the set, $\alpha > 0$ is a scaling factor, and $\delta > 0$ is a pre-defined margin.

B Dataset Details

We provide more details of the CUB-200-2011, Cars196, Stanford Online Products, ImageNet-1K, CIFAR-10, and CIFAR-100 datasets.

For the image retrieval task, we followed existing deep metric learning methods [27, 53, 67, 87] to conduct experiments on the CUB-200-2011 [63], Cars196 [29], and Stanford Online Products [53]. The CUB-200-2011 dataset contains 11,788 images of 200 bird species. We used the first 100 species with 5,864 images for training and the rest 100 species with 5,924 images are for testing. The Cars196 dataset includes 16,183 images of 196 car models. We used the

Table 4: Analysis of the batch size (BS) on the CUB-200-2011 and Cars196 datasets.

BS	CUB-200-2011				Cars196			
	R@1	NMI	RP	M@R	R@1	NMI	RP	M@R
40	66.3	70.6	36.6	25.8	88.2	74.1	41.0	31.8
60	67.1	71.3	36.8	25.9	88.9	75.3	41.6	32.8
80	68.5	72.0	38.3	27.5	89.6	75.6	41.8	32.8
100	69.6	72.5	38.6	27.7	90.0	76.3	42.2	33.3
120	70.7	73.5	39.3	28.4	90.6	76.9	42.6	33.8
140	70.5	73.2	39.3	28.3	90.5	77.2	42.6	33.7
160	70.7	73.3	39.2	28.5	90.7	76.8	42.5	33.5
180	70.7	73.6	39.1	28.2	90.5	77.5	42.6	33.6

first 96 classes with 8,054 images for training and the rest 98 classes with 8,131 images for testing. The Stanford Online Products dataset is relatively large and contains 120,053 images of 22,634 products. We used the first 11,318 products with 59,551 images in the training set and the rest of 11,318 products with 60,502 images for testing.

For the image classification task, we conducted experiments on the widely used ImageNet-1K [47], CIFAR-10 [30], and CIFAR-100 [30]. The ImageNet-1K dataset contains 1,200,000 training images and 50,000 validation images from to 1,000 categories. The CIFAR-10 and CIFAR-100 datasets comprise the same 50,000 images for training and 10,000 images for validation. CIFAR-10 contains 10 classes with 6,000 images per class while CIFAR-100 further provides more fine-grained labels of 100 classes with 600 images per class.

C Further Experimental Analysis

C.1 Effect of the Batch Size

We conducted experiments on the CUB-200-2011 [63] and Cars196 [29] datasets to investigate the influence of the batch size during training. Specifically, we set the batch size from 40 to 180, as shown in Table 4. We observe a relatively consistent performance improvement as the batch size increases on both datasets. This is because larger batch sizes enable richer relation mining among data. Still, we see that the performance plateaus and even decreases when the batch sizes exceed 120. Therefore, we set the batch size to 120 for the main experiments for a better balance of performance and computation.

C.2 Effect of Embedding Sizes

The dimension of the embedding is a crucial factor for the final performance, as verified by several works [27, 89]. During training, the proposed IDML framework simultaneously obtains a semantic embedding and an uncertainty embedding for

Table 5: Analysis of the semantic embedding (SE) size on the CUB-200-2011 and Cars196 datasets.

	CUB-200-2011				Cars196			
SE Size	R@1	NMI	RP	M@R	R@1	NMI	RP	M@R
32	56.9	64.0	32.4	21.6	76.8	68.0	34.1	23.5
64	63.1	67.2	34.8	23.8	83.1	70.6	36.8	26.9
128	66.4	70.2	36.8	26.1	86.0	73.7	39.1	29.6
256	68.5	71.7	37.5	26.5	89.2	76.1	41.1	32.1
512	70.7	73.5	39.3	28.4	90.6	76.9	42.6	33.8
1024	71.0	73.6	39.2	28.4	90.3	76.4	42.7	33.7

Table 6: Analysis of the uncertainty embedding (UE) size on the CUB-200-2011 and Cars196 datasets.

	CUB-200-2011				Cars196			
UE Size	R@1	NMI	RP	M@R	R@1	NMI	RP	M@R
32	69.4	72.5	38.6	27.9	89.2	75.9	41.5	32.5
64	69.2	72.9	38.8	27.6	89.8	76.5	42.3	33.3
128	69.5	73.3	38.8	28.1	89.8	76.7	42.2	33.2
256	70.0	73.2	39.0	28.1	90.1	76.8	42.5	33.6
512	70.7	73.5	39.3	28.4	90.6	76.9	42.6	33.8
1024	70.4	73.4	39.3	28.3	90.4	76.7	42.8	33.9

each image. During testing, we only use the semantic embeddings for inference, introducing no additional computation cost. Still, the uncertainty embedding influences the training of the semantic embedding and thus affects the inference performance.

We first fixed the dimension of the uncertainty embeddings to 512 and used the dimension of 32, 64, 128, 256, 512, and 1024 for the semantic embeddings as shown in Table 5. We observe that the performance improves as the size of the semantic embedding increases and reaches the top at 512 and 1024. We also see that using a dimension of 1024 does not prominently enhance the results, which might result from the information redundancy.

Furthermore, we fixed the semantic embedding size to 512 and tested the performance using the dimension of 32, 64, 128, 256, 512, and 1024 for the uncertainty embeddings, as shown in Table 6. We see that the performance gradually improves as the uncertainty embedding size increases, and the model achieves the best result when the dimension is 512. In summary, we find that using the dimension of 512 for both the semantic embeddings and the uncertainty embeddings achieves the best accuracy/computation trade-off, and we thus adopted them in the main experiments.

Table 7: Effect of different metric formulations.

Datasets	Training Metric	R@1	R@2	NMI	RP	M@R
CUB-200-2011	Euclidean	69.0	79.4	72.3	38.5	27.5
	ISM-Dis (20)	69.2	78.8	72.0	38.7	28.1
	ISM-Sim (19)	70.7	80.2	73.5	39.3	28.4
Cars196	Euclidean	87.3	92.7	75.7	40.9	31.8
	ISM-Dis (20)	89.4	94.0	75.4	41.6	32.5
	ISM-Sim (19)	90.6	94.5	76.9	42.6	33.8

Table 8: Effect of using introspective similarity metric during testing.

Datasets	Testing Metric	R@1	R@2	NMI	RP	M@R
CUB-200-2011	Euclidean (baseline)	69.0	79.4	72.3	38.5	27.5
	ISM (IDML)	69.8	79.6	73.1	39.0	27.8
	Euclidean (IDML)	70.7	80.2	73.5	39.3	28.4
Cars196	Euclidean (baseline)	87.3	92.7	75.7	40.9	31.8
	ISM (IDML)	89.9	93.9	76.2	42.3	33.3
	Euclidean (IDML)	90.6	94.5	76.9	42.6	33.8

C.3 Effect of the Metric Formulation during Training

When uncertain, the proposed metric tends to treat the pair similarly since we think an uncertain metric should not be able to differentiate all pairs. The proposed introspective similarity metric (ISM-Sim) based on the cosine similarity is defined as follows:

$$C_{IN}(\mathbf{x}_i, \mathbf{p}_j) = 1 - (1 - C(\mathbf{x}_i, \mathbf{p}_j)) \cdot e^{(-\frac{1}{\tau} \text{r_conf}(\mathbf{x}_i, \mathbf{p}_j))}. \quad (19)$$

Alternatively, we may also weaken the similarity judgment by encouraging the metric to output large distances to all uncertainty pairs. As a comparison, we additionally modified the metric to treat each ambiguous pair dissimilar (ISM-Dis) as follows:

$$C_{IN}(\mathbf{x}_i, \mathbf{p}_j) = C(\mathbf{x}_i, \mathbf{p}_j) \cdot e^{(-\frac{1}{\tau} \text{r_conf}(\mathbf{x}_i, \mathbf{p}_j))}. \quad (20)$$

We conducted experiments on the CUB-200-2011 and Cars196 datasets to test the performances of using different metric formulations for training in Table 7. We observe that treating each ambiguous pair dissimilar performs worse than the original metric. This verifies our motivation for using uncertainty to weaken the semantic discrepancy.

C.4 Effect of the Metric Formulation during Testing

During testing, we adopt the original similarity metric without our uncertainty-aware term. As an alternative, we conducted an experiment using the introspective similarity metric (ISM) during testing on the CUB-200-2011 and Cars196

Table 9: Application of IDML on vision transformers.

Network	#Param.	FLOPs	Image Size	Top-1 Acc
DeiT-Ti [59]	5M	1.3G	224×224	72.2
DeiT-Ti-IDML	5M	1.3G	224×224	72.7 (+0.5)
DeiT-S [59]	22M	4.6G	224×224	79.8
DeiT-S-IDML	22M	4.6G	224×224	80.5 (+0.7)

datasets, as shown in Table 8. We observe a decrease in performance when using ISM during testing, indicating a harmful effect of using uncertainty to weaken the similarity discrepancy during inference. This is reasonable since providing a clear and confident similarity judgment is probably more beneficial to discriminative tasks such as image classification.

C.5 Application of IDML on Different Backbone Architectures

We applied our IDML framework to different backbone architectures to show its generalization. Given the recent success of Vision Transformers (ViTs) [12], we adopt DeiT [59] as the backbone model. ViTs first formulate each image into a sequence of patches and flatten them to construct patch tokens. They additionally use a class token to extract the image-level feature. To apply the proposed IDML framework to ViTs, we further employ an uncertainty token for uncertainty measure. We treat the output class token and uncertainty token as the semantic embedding and uncertainty embedding, respectively. We then employ the proposed ISM to replace the cosine similarity in the classifier and use the same softmax loss during training. We discard the uncertainty token during inference and use the same architecture as the original transformer without extra computation cost. The experimental results are shown in Table 9. We observe consistent performance boosts with relatively large margins when applying IDML to both DeiT-Tiny and DeiT-Small, showing the universality of IDML. We will apply our framework to more architectures in the future.

C.6 Comparisons of Different Training Recipes for ResNet-50

We provide detailed comparisons of different training recipes for ResNet-50 in Table 10 following [70]. We instantiate our framework using a vanilla setting since the main objective is to evaluate the effectiveness of using the proposed metric for training. We see that our IDML achieves very competitive performance despite using a very constrained setting (*e.g.*, a small batch size). In particular, we outperform CutMix [78] using the same hyperparameters. Several recipes achieve better performances including FAMS [11], Timm-A1 [70], and Timm-A2 [70]. However, they all use a larger batch size (at least $4\times$ than our setting) and a more advanced data augmentation strategy. FAMS [11] and Timm-A1 [70] further train more epochs to achieve better performance. In contrast, our framework achieves competitive performance without bells and whistles. We will train our framework using better-performing recipes in the future.

Table 10: Comparisons of different training recipes for ResNet-50. Part of this table is derived from [70].

Procedure → Reference	PyTorch [41]	DeiT [59]	FAMS (×4) [11]	Timm-A1 [70]	Timm-A2 [70]	Timm-A3 [70]	ConvNet [32]	CutMix [78]	Ours
Train Res	224	224	224	224	224	160	224	224	224
Test Res	224	224	224	224	224	224	224	224	224
Epochs	90	300	400	600	300	100	300	300	300
Batch size	256	1024	1024	2048	2048	2048	4096	256	256
Optimizer	SGD-M	AdamW	SGD-M	LAMB	LAMB	LAMB	AdamW	SGD-M	SGD-M
LR	0.1	1×10^{-3}	2.0	5×10^{-3}	5×10^{-3}	8×10^{-3}	4×10^{-3}	0.1	0.1
LR decay	step	cosine	step	cosine	cosine	cosine	cosine	step	step
Weight decay	10^{-4}	0.05	10^{-4}	0.01	0.02	0.02	0.05	10^{-4}	10^{-4}
Warmup epochs	×	5	5	5	5	5	20	×	×
Label smoothing ε	×	0.1	0.1	0.1	×	×	0.1	×	×
Stoch. Depth	×	0.1	×	0.05	0.05	×	0.1	×	×
Repeated Aug	×	✓	×	✓	✓	×	×	×	×
Gradient Clip.	×	×	×	×	×	×	×	×	×
H. flip	✓	✓	✓	✓	✓	✓	✓	✓	✓
RRC	✓	✓	✓	✓	✓	✓	✓	✓	✓
Rand Augment	×	9/0.5	×	7/0.5	7/0.5	6/0.5	9/0.5	×	×
Auto Augment	×	×	✓	×	×	×	×	×	×
Mixup alpha	×	0.8	0.2	0.2	0.1	0.1	0.8	×	×
Cutmix alpha	×	1.0	×	1.0	1.0	1.0	1.0	1.0	1.0
Erasing prob.	×	0.25	×	×	×	×	0.25	×	×
ColorJitter	✓	×	×	×	×	×	×	×	×
PCA lighting	×	×	×	×	×	×	×	×	×
SWA	×	×	✓	×	×	×	×	×	×
EMA	×	×	×	×	×	×	×	×	×
Test crop ratio	0.875	0.875	0.875	0.95	0.95	0.95	1.0	0.875	0.875
CE loss	✓	✓	✓	×	×	×	✓	✓	✓
BCE loss	×	×	×	✓	✓	✓	×	×	×
Introspective metric	×	×	×	×	×	×	×	×	✓
Top-1 acc.	76.1%	78.4%	79.5%	80.4%	79.8%	78.1%	78.8%	78.6%	79.0%

Bibliography

- [1] Babenko, A., Slesarev, A., Chigorin, A., Lempitsky, V.: Neural codes for image retrieval. In: ECCV. pp. 584–599 (2014) [1](#)
- [2] Cakir, F., He, K., Xia, X., Kulis, B., Sclaroff, S.: Deep metric learning to rank. In: CVPR. pp. 1861–1870 (2019) [3](#), [9](#), [11](#)
- [3] Chang, J., Lan, Z., Cheng, C., Wei, Y.: Data uncertainty learning in face recognition. In: CVPR. pp. 5710–5719 (2020) [3](#)
- [4] Chen, T., Kornblith, S., Norouzi, M., Hinton, G.: A simple framework for contrastive learning of visual representations. In: ICML. pp. 1597–1607 (2020) [1](#)
- [5] Chen, W., Chen, X., Zhang, J., Huang, K.: Beyond triplet loss: a deep quadruplet network for person re-identification. In: CVPR. pp. 1320–329 (2017) [11](#)
- [6] Chen, X., He, K.: Exploring simple siamese representation learning. In: CVPR. pp. 15750–15758 (2021) [1](#)
- [7] Chou, H.P., Chang, S.C., Pan, J.Y., Wei, W., Juan, D.C.: Remix: Rebalanced mixup. In: ECCV. pp. 95–110 (2020) [2](#)
- [8] Chun, S., Oh, S.J., de Rezende, R.S., Kalantidis, Y., Larlus, D.: Probabilistic embeddings for cross-modal retrieval. In: CVPR. pp. 8415–8424 (2021) [2](#), [4](#)
- [9] Deng, J., Guo, J., Xue, N., Zafeiriou, S.: Arcface: Additive angular margin loss for deep face recognition. In: CVPR. pp. 4690–4699 (2019) [1](#), [3](#), [7](#)
- [10] Do, T.T., Tran, T., Reid, I., Kumar, V., Hoang, T., Carneiro, G.: A theoretically sound upper bound on the triplet loss for improving the efficiency of deep distance metric learning. In: CVPR. pp. 10404–10413 (2019) [3](#)
- [11] Dollár, P., Singh, M., Girshick, R.: Fast and accurate model scaling. In: CVPR. pp. 924–932 (2021) [12](#), [20](#), [21](#)
- [12] Dosovitskiy, A., Beyer, L., Kolesnikov, A., Weissenborn, D., Zhai, X., Unterthiner, T., Dehghani, M., Minderer, M., Heigold, G., Gelly, S., et al.: An image is worth 16x16 words: Transformers for image recognition at scale. In: ICLR (2020) [20](#)
- [13] Duan, Y., Zheng, W., Lin, X., Lu, J., Zhou, J.: Deep adversarial metric learning. In: CVPR. pp. 2780–2789 (2018) [3](#), [6](#)
- [14] Grill, J.B., Strub, F., Althé, F., Tallec, C., Richemond, P., Buchatskaya, E., Doersch, C., Avila Pires, B., Guo, Z., Gheshlaghi Azar, M., et al.: Bootstrap your own latent-a new approach to self-supervised learning. In: NeurIPS. pp. 21271–21284 (2020) [1](#)
- [15] Guo, S., Xu, J., Chen, D., Zhang, C., Wang, X., Zhao, R.: Density-aware feature embedding for face clustering. In: CVPR. pp. 6698–6706 (2020) [1](#)
- [16] Han, D., Kim, J., Kim, J.: Deep pyramidal residual networks. In: CVPR. pp. 5927–5935 (2017) [10](#)
- [17] Harwood, B., Kumar B G, V., Carneiro, G., Reid, I., Drummond, T.: Smart mining for deep metric learning. In: ICCV. pp. 2840–2848 (2017) [3](#)

- [18] He, K., Fan, H., Wu, Y., Xie, S., Girshick, R.: Momentum contrast for unsupervised visual representation learning. In: CVPR. pp. 9729–9738 (2020) [1](#)
- [19] He, K., Zhang, X., Ren, S., Sun, J.: Deep residual learning for image recognition. In: CVPR. pp. 770–778 (2016) [2](#), [10](#), [11](#)
- [20] Hershey, J.R., Olsen, P.A.: Approximating the kullback leibler divergence between gaussian mixture models. In: ICASSP. pp. IV–317 (2007) [2](#), [4](#)
- [21] Hinton, G., Vinyals, O., Dean, J., et al.: Distilling the knowledge in a neural network. In: NeurIPS (2015) [5](#)
- [22] Hu, J., Lu, J., Tan, Y.P.: Discriminative deep metric learning for face verification in the wild. In: CVPR. pp. 1875–1882 (2014) [3](#), [4](#), [9](#), [11](#), [15](#)
- [23] Ioffe, S., Szegedy, C.: Batch normalization: Accelerating deep network training by reducing internal covariate shift. In: ICLR. pp. 448–456 (2015) [11](#)
- [24] Jacob, P., Picard, D., Histace, A., Klein, E.: Metric learning with horde: High-order regularizer for deep embeddings. In: ICCV (2019) [9](#)
- [25] Kemertas, M., Pishdad, L., Derpanis, K.G., Fazly, A.: Rankmi: A mutual information maximizing ranking loss. In: CVPR. pp. 14362–14371 (2020) [9](#)
- [26] Kendall, A., Gal, Y.: What uncertainties do we need in bayesian deep learning for computer vision? In: NeurIPS. pp. 5574–5584 (2017) [3](#)
- [27] Kim, S., Kim, D., Cho, M., Kwak, S.: Proxy anchor loss for deep metric learning. In: CVPR. pp. 3238–3247 (2020) [3](#), [9](#), [11](#), [16](#), [17](#)
- [28] Ko, B., Gu, G., Kim, H.G.: Learning with memory-based virtual classes for deep metric learning. In: ICCV. pp. 11792–11801 (2021) [9](#)
- [29] Krause, J., Stark, M., Deng, J., Fei-Fei, L.: 3d object representations for fine-grained categorization. In: ICCVW. pp. 554–561 (2013) [10](#), [11](#), [16](#), [17](#)
- [30] Krizhevsky, A., Hinton, G., et al.: Learning multiple layers of features from tiny images (2009) [10](#), [11](#), [17](#)
- [31] Li, W., Huang, X., Lu, J., Feng, J., Zhou, J.: Learning probabilistic ordinal embeddings for uncertainty-aware regression. In: CVPR. pp. 13896–13905 (2021) [3](#)
- [32] Liu, Z., Mao, H., Wu, C.Y., Feichtenhofer, C., Darrell, T., Xie, S.: A convnet for the 2020s. arXiv [abs/2201.03545](#) (2022) [12](#), [21](#)
- [33] Milbich, T., Roth, K., Bharadhwaj, H., Sinha, S., Bengio, Y., Ommer, B., Cohen, J.P.: Diva: Diverse visual feature aggregation for deep metric learning. In: ECCV. pp. 590–607 (2020) [9](#)
- [34] Mohan, D.D., Sankaran, N., Fedorishin, D., Setlur, S., Govindaraju, V.: Moving in the right direction: A regularization for deep metric learning. In: CVPR. pp. 14591–14599 (2020) [9](#)
- [35] Movshovitz-Attias, Y., Toshev, A., Leung, T.K., Ioffe, S., Singh, S.: No fuss distance metric learning using proxies. In: ICCV. pp. 360–368 (2017) [3](#), [4](#), [9](#), [11](#), [15](#)
- [36] Musgrave, K., Belongie, S., Lim, S.N.: A metric learning reality check. In: ECCV (2020) [10](#)
- [37] Neelakantan, A., Shankar, J., Passos, A., McCallum, A.: Efficient non-parametric estimation of multiple embeddings per word in vector space. In: EMNLP. pp. 1059–1069 (2014) [3](#)

- [38] Nguyen, D.Q., Nguyen, D.Q., Modi, A., Thater, S., Pinkal, M.: A mixture model for learning multi-sense word embeddings. arXiv **abs/1706.05111** (2017) **3**
- [39] Nguyen, H.V., Bai, L.: Cosine similarity metric learning for face verification. In: ACCV. pp. 709–720 (2010) **6**
- [40] Oh, S.J., Murphy, K.P., Pan, J., Roth, J., Schroff, F., Gallagher, A.C.: Modeling uncertainty with hedged instance embeddings. In: ICLR (2018) **2, 3, 4, 11, 12**
- [41] Paszke, A., Gross, S., Massa, F., Lerer, A., Bradbury, J., Chanan, G., Killeen, T., Lin, Z., Gimelshein, N., Antiga, L., et al.: Pytorch: An imperative style, high-performance deep learning library. In: NeurIPS. pp. 8026–8037 (2019) **9, 21**
- [42] Qi, Q., Yan, Y., Wu, Z., Wang, X., Yang, T.: A simple and effective framework for pairwise deep metric learning. In: ECCV (2020) **9**
- [43] Qian, Q., Shang, L., Sun, B., Hu, J.: Softtriple loss: Deep metric learning without triplet sampling. In: ICCV. pp. 6450–6458 (2019) **9**
- [44] Roth, K., Brattoli, B., Ommer, B.: Mic: Mining interclass characteristics for improved metric learning. In: ICCV. pp. 8000–8009 (2019) **9**
- [45] Roth, K., Milbich, T., Ommer, B.: Pads: Policy-adapted sampling for visual similarity learning. In: CVPR. pp. 6568–6577 (2020) **9**
- [46] Roth, K., Vinyals, O., Akata, Z.: Non-isotropy regularization for proxy-based deep metric learning. In: CVPR (2022) **9**
- [47] Russakovsky, O., Deng, J., Su, H., Krause, J., Satheesh, S., Ma, S., Huang, Z., Karpathy, A., Khosla, A., Bernstein, M., et al.: Imagenet large scale visual recognition challenge. IJCV **115**(3), 211–252 (2015) **10, 11, 17**
- [48] Sanakoyeu, A., Ma, P., Tschernezki, V., Ommer, B.: Improving deep metric learning by divide and conquer. TPAMI (2021) **9**
- [49] Schroff, F., Kalenichenko, D., Philbin, J.: Facenet: A unified embedding for face recognition and clustering. In: CVPR. pp. 815–823 (2015) **1, 2, 3, 9, 11, 15**
- [50] Shaw, G., Manolakis, D.: Signal processing for hyperspectral image exploitation. SPM **19**(1), 12–16 (2002) **3**
- [51] Shi, Y., Jain, A.K.: Probabilistic face embeddings. In: ICCV. pp. 6902–6911 (2019) **1, 3**
- [52] Simonyan, K., Zisserman, A.: Very deep convolutional networks for large-scale image recognition. arXiv **abs/1409.1556** (2014) **2**
- [53] Song, H.O., Xiang, Y., Jegelka, S., Savarese, S.: Deep metric learning via lifted structured feature embedding. In: CVPR. pp. 4004–4012 (2016) **1, 3, 9, 10, 11, 16**
- [54] Sun, J.J., Zhao, J., Chen, L.C., Schroff, F., Adam, H., Liu, T.: View-invariant probabilistic embedding for human pose. In: ECCV. pp. 53–70 (2020) **2, 4**
- [55] Sun, Y., Cheng, C., Zhang, Y., Zhang, C., Zheng, L., Wang, Z., Wei, Y.: Circle loss: A unified perspective of pair similarity optimization. In: CVPR. pp. 6398–6407 (2020) **7, 9**

- [56] Szegedy, C., Liu, W., Jia, Y., Sermanet, P., Reed, S.E., Anguelov, D., Erhan, D., Vanhoucke, V., Rabinovich, A.: Going deeper with convolutions. In: CVPR. pp. 1–9 (2015) **2**
- [57] Tang, L., Wertheimer, D., Hariharan, B.: Revisiting pose-normalization for fine-grained few-shot recognition. In: CVPR. pp. 14352–14361 (2020) **1**
- [58] Teh, E.W., DeVries, T., Taylor, G.W.: Proxynca++: Revisiting and revitalizing proxy neighborhood component analysis. In: ECCV (2020) **9**
- [59] Touvron, H., Cord, M., Douze, M., Massa, F., Sablayrolles, A., Jégou, H.: Training data-efficient image transformers & distillation through attention. In: ICML. pp. 10347–10357 (2021) **14, 20, 21**
- [60] Van Der Maaten, L.: Accelerating t-sne using tree-based algorithms. JMLR **15**(1), 3221–3245 (2014) **13, 14**
- [61] Verma, V., Lamb, A., Beckham, C., Najafi, A., Mitliagkas, I., Lopez-Paz, D., Bengio, Y.: Manifold mixup: Better representations by interpolating hidden states. In: ICLR. pp. 6438–6447 (2019) **2**
- [62] Vilnis, L., McCallum, A.: Word representations via gaussian embedding. In: ICLR (2015) **3**
- [63] Wah, C., Branson, S., Welinder, P., Perona, P., Belongie, S.J.: The Caltech-UCSD Birds-200-2011 dataset. Tech. Rep. CNS-TR-2011-001, California Institute of Technology (2011) **10, 11, 16, 17**
- [64] Wang, H., Wang, Y., Zhou, Z., Ji, X., Gong, D., Zhou, J., Li, Z., Liu, W.: Cosface: Large margin cosine loss for deep face recognition. In: CVPR. pp. 5265–5274 (2018) **3**
- [65] Wang, J., Zhou, F., Wen, S., Liu, X., Lin, Y.: Deep metric learning with angular loss. In: ICCV. pp. 2593–2601 (2017)
- [66] Wang, J., Song, Y., Leung, T., Rosenberg, C., Wang, J., Philbin, J., Chen, B., Wu, Y.: Learning fine-grained image similarity with deep ranking. In: CVPR. pp. 1386–1393 (2014)
- [67] Wang, X., Han, X., Huang, W., Dong, D., Scott, M.R.: Multi-similarity loss with general pair weighting for deep metric learning. In: CVPR. pp. 5022–5030 (2019) **3, 9, 11, 16**
- [68] Wang, X., Zhang, H., Huang, W., Scott, M.R.: Cross-batch memory for embedding learning. In: CVPR. pp. 6388–6397 (2020) **1**
- [69] Wertheimer, D., Tang, L., Hariharan, B.: Few-shot classification with feature map reconstruction networks. In: CVPR. pp. 8012–8021 (2021) **1**
- [70] Wightman, R., Touvron, H., Jégou, H.: Resnet strikes back: An improved training procedure in timm. arXiv **abs/2110.00476** (2021) **12, 20, 21**
- [71] Wu, C.Y., Manmatha, R., Smola, A.J., Krähenbühl, P.: Sampling matters in deep embedding learning. In: ICCV. pp. 2859–2867 (2017) **2, 3, 7, 9, 11**
- [72] Yang, L., Zhan, X., Chen, D., Yan, J., Loy, C.C., Lin, D.: Learning to cluster faces on an affinity graph. In: CVPR. pp. 2298–2306 (2019) **1**
- [73] Ye, M., Shen, J.: Probabilistic structural latent representation for unsupervised embedding. In: CVPR. pp. 5457–5466 (2020) **4**
- [74] Yu, B., Tao, D.: Deep metric learning with tuplet margin loss. In: ICCV. pp. 6490–6499 (2019) **3**

- [75] Yu, D., Yao, K., Su, H., Li, G., Seide, F.: Kl-divergence regularized deep neural network adaptation for improved large vocabulary speech recognition. In: ICASSP. pp. 7893–7897 (2013) [4](#)
- [76] Yuan, T., Deng, W., Tang, J., Tang, Y., Chen, B.: Signal-to-noise ratio: A robust distance metric for deep metric learning. In: CVPR. pp. 4815–4824 (2019) [6](#)
- [77] Yuan, Y., Yang, K., Zhang, C.: Hard-aware deeply cascaded embedding. In: ICCV. pp. 814–823 (2017) [3](#)
- [78] Yun, S., Han, D., Oh, S.J., Chun, S., Choe, J., Yoo, Y.: Cutmix: Regularization strategy to train strong classifiers with localizable features. In: ICCV. pp. 6023–6032 (2019) [3](#), [6](#), [10](#), [11](#), [20](#), [21](#)
- [79] Zhang, B., Wonka, P.: Point cloud instance segmentation using probabilistic embeddings. In: CVPR. pp. 8883–8892 (2021) [2](#), [3](#)
- [80] Zhang, B., Zheng, W., Zhou, J., Lu, J.: Attributable visual similarity learning. In: CVPR (2022) [3](#)
- [81] Zhang, D., Li, Y., Zhang, Z.: Deep metric learning with spherical embedding. *NeurIPS* **33**, 18772–18783 (2020) [9](#)
- [82] Zhang, H., Cisse, M., Dauphin, Y.N., Lopez-Paz, D.: mixup: Beyond empirical risk minimization. In: ICLR (2018) [2](#), [3](#), [6](#), [7](#), [10](#)
- [83] Zhang, L., Xiang, T., Gong, S.: Learning a deep embedding model for zero-shot learning. In: CVPR. pp. 2021–2030 (2017) [2](#)
- [84] Zhao, W., Rao, Y., Wang, Z., Lu, J., Zhou, J.: Towards interpretable deep metric learning with structural matching. In: CVPR. pp. 9887–9896 (2021) [9](#)
- [85] Zheng, W., Lu, J., Jie, Z.: Structural deep metric learning for room layout estimation. In: ECCV (2020) [3](#)
- [86] Zheng, W., Lu, J., Zhou, J.: Deep metric learning via adaptive learnable assessment. In: CVPR. pp. 2960–2969 (2020) [3](#)
- [87] Zheng, W., Lu, J., Zhou, J.: Hardness-aware deep metric learning. *TPAMI* (2020) [3](#), [16](#)
- [88] Zheng, W., Wang, C., Lu, J., Zhou, J.: Deep compositional metric learning. In: CVPR. pp. 9320–9329 (2021) [1](#), [9](#)
- [89] Zheng, W., Zhang, B., Lu, J., Zhou, J.: Deep relational metric learning. In: CVPR. pp. 12065–12074 (2021) [9](#), [17](#)
- [90] Zhu, H., Yuan, Y., Hu, G., Wu, X., Robertson, N.: Imbalance robust softmax for deep embedding learning. In: ACCV (2020) [1](#)
- [91] Zhu, Y., Yang, M., Deng, C., Liu, W.: Fewer is more: A deep graph metric learning perspective using fewer proxies. In: *NeurIPS*. pp. 17792–17803 (2020) [9](#)